GEOPHYSICAL RESEARCH LETTERS, VOL. 35, L21306, doi:10.1029/2008GL035614, 2008

Heterogeneous Coulomb stress perturbation during earthquake cycles in a 3D rate-and-state fault model

F. Gallovič[1]

Received 8 August 2008; revised 7 October 2008; accepted 9 October 2008; published 11 November 2008.

[1] We perform a numerical experiment with quasi-dynamic continuous 3D fault model governed by a laboratory derived rate-and-state friction law. We test several cases in which the Coulomb stress (CS) increases either on the whole fault or only on its part. For the partial stressing we find that if the triggering is almost instantaneous (within 1–2 months), the nucleation takes place in the strike extent of the CS increase area. On the contrary, if the earthquake does not occur within these few months, it can nucleate anywhere on the fault, and even later than without the positive CS load. These features represent new findings which are unique for 3D model and cannot be explained by 1D spring-slider models. The finding might find applications in the aftershock (time-dependent) seismic hazard assessment. **Citation:** Gallovič, F. (2008), Heterogeneous Coulomb stress perturbation during earthquake cycles in a 3D rate-and-state fault model, *Geophys. Res. Lett.*, *35*, L21306, doi:10.1029/2008GL035614.

1. Introduction

[2] Earthquake triggering due to the Coulomb stress (CS) transfer is a well documented phenomenon in seismic active areas [see, e.g., *Steacy et al.*, 2005, and references therein]. The CS change ΔCS is a combination of change in normal stress $\Delta\sigma$ and traction $\Delta\tau$ in the slip direction,

$$\Delta CS = \Delta\tau - \mu\Delta\sigma, \tag{1}$$

where μ is a coefficient of friction. Generally, a positive CS change is considered to bring the fault closer to the failure, while a negative one to delay the earthquake occurrence. Recently, attempts have been made to study the CS triggering for various earthquake fault models [*Dieterich*, 1994; *Gomberg et al.*, 1998; *Roy and Marone*, 1996].

[3] In particular, *Perfettini et al.* [2003] performed a numerical study on CS triggering using 2D rate-and-state fault model explaining the clock advance of the earthquake occurrence due to positive CS change. For example, *Perfettini et al.* [2003] found oscillatory behavior of the clock advance as a function of CS load time around a mean value that is in agreement with simple Coulomb failure model. Note that the CS load was applied on the whole fault and no emphasis was put on the effect of CS on nucleation of the earthquake instability.

[4] In the present paper the study by *Perfettini et al.* [2003] is extended utilizing quasi-dynamic continuous 3D fault model governed by a laboratory derived rate-and-state friction law [*Dieterich*, 1979; *Rice*, 1993]. Besides applying the CS increase on the whole fault, we also apply it on parts of the fault only. Note that the latter cases do not have simple equivalents in the spring-slider models [*Roy and Marone*, 1996], and, therefore, have to be solved numerically. We pay attention to the spatial relation between the area of the CS increase on the fault and the nucleation point position. This is important for seismic hazard assessment, since ground motion estimates are highly sensitive to the nucleation point position.

2. Modeling Approach

[5] We assume a vertical strike-slip 3D fault discretized into $N_L \times N_W$ cells, constantly driven by a plate motion. At any time step t, frictional stress τ_i at fault cell i equals the product of normal stress $\sigma_i(t)$ and friction coefficient μ_i that itself depends on slip velocity $V_i(t)$ and state variable $\theta_i(t)$

$$\tau_i(V_i(t),\theta_i(t),\sigma_i(t)) = \sigma_i(t)\mu_i(V_i(t),\theta_i(t)). \tag{2}$$

[6] We utilize the laboratory-derived rate- and state-dependent coefficient of friction [*Dieterich*, 1979; *Ruina*, 1983], which successfully explains numerous earthquake phenomena [*Scholz*, 1998]. It reads

$$\mu_i(V_i(t),\theta_i(t)) = \mu^* + a_i \ln\left(V_i(t)/V^*\right) + b_i \ln\left(\theta_i(t)V^*/D_c\right), \tag{3}$$

where μ^* is the friction coefficient at reference velocity V^*, a_i and b_i are governing parameters and D_c is the characteristic friction distance. The state variable θ_i evolves as [*Linker and Dieterich*, 1992]

$$\frac{d\theta_i(t)}{dt} = 1 - \frac{V_i\theta_i}{D_c} - \frac{\alpha_i\theta_i}{b_i}\frac{\dot\sigma_i}{\sigma_i}, \tag{4}$$

where parameter α_i controls the state variable response to temporal change in normal stress σ_i.

[7] The frictional stress has to satisfy the shear stress condition on the fault

$$\tau_i(V_i(t),\theta_i(t),\sigma_i(t)) = \tau^0 - \frac{G}{2\beta}\left(V_i(t) - V^{pl}\right) + \sum_{j=1}^{N_L N_W} K_{ij}\left(d_j(t) - V^{pl}t\right) + \Delta\tau_i(t), \tag{5}$$

where τ^0 is the initial stress, V^{pl} represents the loading plate velocity, d_j denotes the slip at cell j and $\Delta\tau_i$ the stress change due to external source. Parameters G and β are shear

[1]Department of Geophysics, Faculty of Mathematics and Physics, Charles University in Prague, Prague, Czech Republic.

0094-8276/08/2008GL035614$05.00

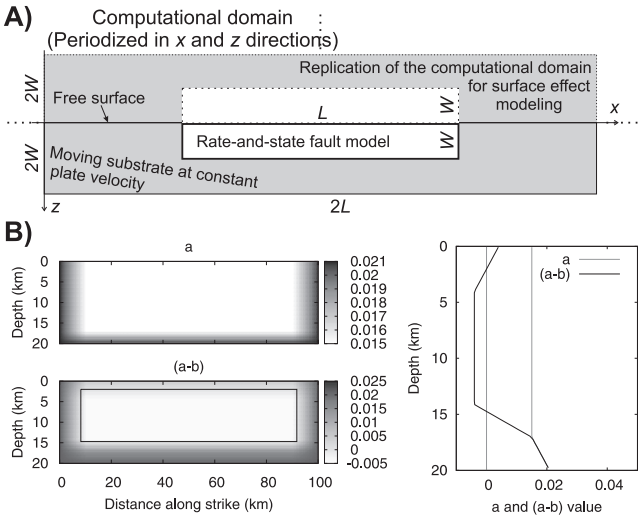

Figure 1. (a) Rate-and-state controlled vertical strike-slip fault (white bold rectangle) in 3D elastic halfspace. The computation domain extends twice the fault length and twice the fault width (solid gray rectangle). The computation is further replicated in the dip direction to account for the free surface effect (dashed rectangles). Due to the use of Fast Fourier Transform in evaluation of the stress distribution, the whole computational domain is in fact replicated in both along strike and along dip directions. Due to the zero-padding the replications do not influence the actual fault evolution. (b) Distribution of (left) a and (a-b) values on the fault and (right) their depth cross-section through the middle of the fault. The inner rectangle in Figure 1b (left) represents a boundary between the velocity weakening ($b > a$, inside the rectangle) and strengthening ($b < a$, outside the rectangle) fault area.

modulus and S-wave velocity, respectively. The second term on the right side imposes the radiation damping [*Rice*, 1993]. Kernel K_{ij} accounts for the static part of the dynamic elastic interactions among the cells (hence quasi-dynamic approach). *Perfettini et al.* [2003] derived this kernel for 2D antiplane fault. Here we use kernel that we have derived in analogous way but for 3D infinite homogeneous isotropic elastic medium (characterized by Lamé's parameters G and λ) utilizing the representation theorem [*Andrews*, 1974] and assuming that the slip remains in the horizontal (strike) direction during the whole earthquake cycle.

[8] Putting right sides of equations (2) and (5) into equation, differentiating it with respect to time, one arrives after simple algebra to a system of $N_L N_W$ ordinary differential equations

$$\frac{dV_i(t)}{dt} = \frac{\sum_{j=1}^{N_L N_W} K_{ij}\left(V_j - V^{pl}\right) - \sigma_i \dot{\theta}_i(\partial\mu_i/\partial\theta_i) - \mu_i\dot{\sigma}_i + \Delta\dot{\tau}_i}{\sigma_i(\partial\mu_i/\partial V_i) + G/(2\beta)}. \quad (6)$$

[9] Note that the last two terms of the numerator correspond to time derivative of the CS change equation (1) realizing that $\dot{\sigma}_i = \Delta\dot{\sigma}_i$. The system equation (6), after inserting equation (3), together with the other system of $N_L N_W$ (equation (4)), is to be integrated numerically to obtain the temporal evolution of slip velocities $V_i(t)$ and state variables $\theta_i(t)$ along the fault. We use Runge-Kutta algorithm with a fifth-order adaptive step-size control [*Press et al.*, 1992]. The sum in equation (6) can be written as a spatial convolution, and is evaluated by means of the 2D Fast Fourier Transform (FFT). Figure 1a shows the problem geometry together with zero-padding that allows to minimize the effect of artificial replications due to the use of FFT.

[10] All the parameters assumed in our study are listed in Table 1 or shown in Figure 1b. The normal stress σ is kept constant throughout the depth, which corresponds to high fluid overpressurization at depth as discussed by *Rice* [1993]. In our setting friction coefficient μ_i varies between 0.60–0.62. The discretization of the computational domain is dense enough to consider our fault model to be continuous [*Rice*, 1993].

3. Modeling Results

3.1. Regular Earthquake Cycle (No Coulomb Stress Load)

[11] At the beginning the fault is set to the steady state with slip velocities equal to the plate velocity ($V_i = V^{pl}$,$\theta_i = D_c/V^{pl}$). To artificially initiate the fault, we increase 10 times the slip velocity in the center of the fault at time $t = 0$ s. After this initiation, the fault evolves to a plate velocity driven regular cycle, which is characterized by periods of slow stable evolution of slip velocities and state variables, and occasional slip velocity instabilities (earthquakes). For the further discussion, we consider the earthquake to start when the slip velocity reaches a more or less arbitrarily chosen value of 1 mm/s anywhere on the fault. Utilizing this definition, the present fault model produces an earthquake instability regularly every 98 years (Figure 2a).

[12] The fault behaves periodically also in terms of distribution of slip velocities along the fault when approaching the instability (Figure 2b). Figure 2b also shows the position of the nucleation point defined as the point at which the slip velocity first reaches 1 mm/s. Note that in this case the nucleation point is doubled as the slip velocity reaches 1 mm/s simultaneously at two symmetrical points. The earthquake ruptures the whole fault.

[13] As an example, the slip accumulated during the period of 200–500 years is shown in Figure 2c. One can see the repetitive slow slip increase at the sides of the fault (governed by the velocity-strengthening border of the fault with $b < a$, see Figure 1b), and the sudden slip increase

Table 1. Parameters of the Model Under Study

Parameter	Description	Value
L	Fault length	100 km
W	Fault width	20 km
N_L	No. of samples along x-axis	1024
N_W	No. of samples along z-axis	256
G	Shear modulus	30 GPa
λ	Lamé's parameter	20 GPa
β	S-wave velocity	3 km/s
σ	Normal stress	75 MPa
V^{pl}	Plate velocity	3.5 cm/yr
D_c	Characteristic friction distance	2 cm
α_i	State variable parameter	0.2, $b_i > 0$ 0.0, $b_i = 0$
μ^*	Reference coefficient of friction	0.6
V^*	Reference slip velocity	1 μm/s

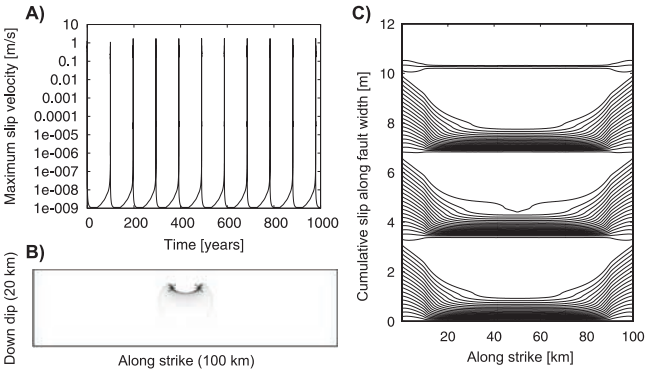

Figure 2. (a) Maximum slip velocity on the fault as a function of time t after the initiation at $t = 0$ yr. The regular earthquake cycle has period of 98 years. (b) Slip velocity snapshot at the time of the nucleation applicable for the third and all later earthquakes after the fault initiation. Stars denote two simultaneous nucleation points. (c) Cumulative slip integrated along the fault width plotted as a function of the along strike distance every 5 years (for the period of 200–500 years). Note the relatively slow creep at sides of the fault and the sudden slip during the earthquake instability.

during the earthquake instabilities in the velocity-weakening part of the fault ($b > a$, see Figure 1b) that balances the slip deficit.

3.2. Homogeneous and Heterogeneous Coulomb Stress Load

[14] Here we disturb the fault from its regular behavior by applying CS load after the earthquake which took place at 392 yr. We test cases in which the CS increases either on the whole fault (homogeneous load) or only on a fault patch (heterogeneous load). The stressed areas are shown in the top of Figure 3a.

[15] We apply the CS increase at various times after 392 yr to study also the influence of the actual stage of the earthquake cycle at which the CS is applied. Figure 3a shows the slip velocity snapshots at the time of the earthquake nucleation together with the nucleation points for various CS load times (rows) and various areas of the CS increase (columns). For simplicity, only increase of the tangential stress by 0.2 MPa or 1.2 MPa in case of homogeneous or patch loads, respectively, is assumed to represent the CS load (equation (1)).

[16] When the whole fault is subject to the CS increase (Figure 3a (left)), the slip velocities along the fault at the time of earthquake nucleation are different than during the regular cycle (Figure 2b) although they remain symmetrical. For some load times the earthquake even ''doubles'', nucleating simultaneously on the two opposite sides of the fault (e.g., for times 430 yr and 485–489 yr).

[17] In cases of the CS increase at parts of the fault (Figures 3a (middle) and 3a (right)), the fault evolution is not symmetrical any more. Early in the seismic cycle, for load times $\leq$470 yr, the earthquake nucleates at various places on the fault, being seemingly not related to the CS increase fault area. On the other hand, later in the earthquake cycle, for load times >470–480 yr, the nucleation point moves to the left part of the fault where the CS increase area is located. Nevertheless, the depth of the nucleation point is not well constrained by the depth of the CS area. Only, as our other test showed, when the CS patch is located exactly in the nucleation zone of the regular cycle, then the actual nucleation point lies in the CS patch for all CS times.

[18] Let us discuss the CS triggering with respect to the earthquake occurrence time. Without any disturbance, the next earthquake would occur at 490 yr during the regular cycle (see Figure 2a). Figure 3b shows the clock advance of the earthquake occurrence as a function of the CS load time. Note that the applied CS load is the same as above. As one can see in Figure 3b, the clock advance is an oscillating function, which is in agreement with the finding by *Perfettini et al.* [2003]. When the CS load is applied to

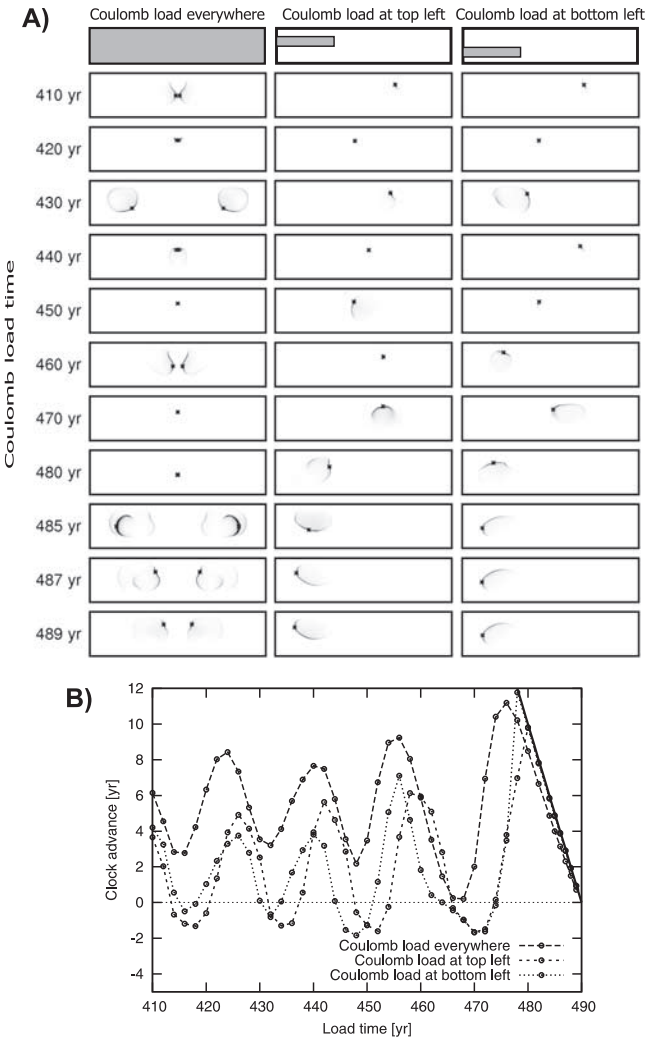

Figure 3. (a) Slip velocity snapshots at the time of earthquake nucleation for various times of the Coulomb load time (rows) and for various Coulomb increase areas on the fault (columns). Stars denote the nucleation points. (b) Clock advance dependence on the Coulomb load time (lines with circles) for the various areas of Coulomb stress increase (see legend). The solid line corresponds to maximum possible (instantaneous) clock advance. Coulomb stress loads are realized by tangential stress increase by 0.2 MPa or 1.2 MPa in case of homogeneous or patch loads, respectively.

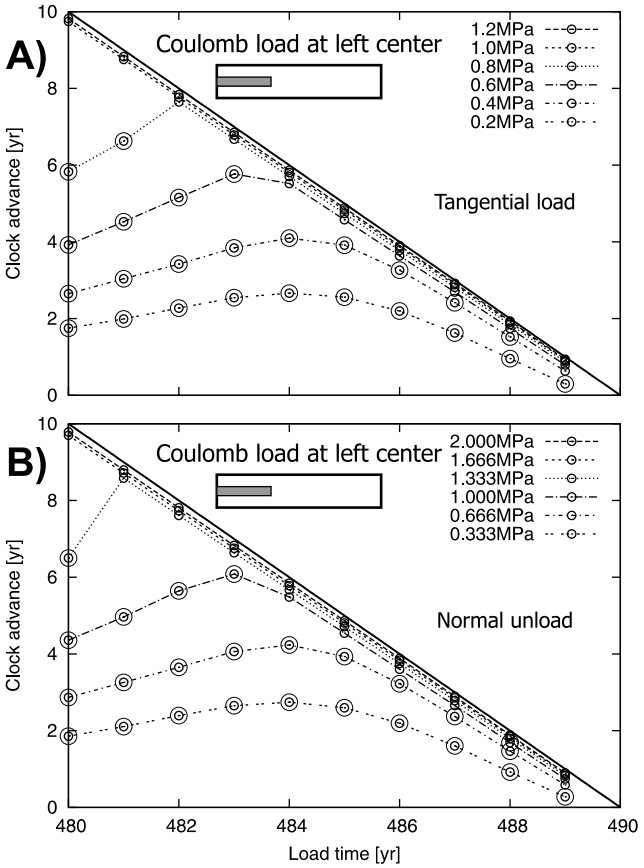

Figure 4. Clock advance as a function of the Coulomb stress load time for last 9 years before the regular earthquake occurrence (dashed lines with small circles). The Coulomb stress change is realized by (a) tangential load or (b) normal unload with various stress amplitudes (see legend). Note that the normal stress unloads, when multiplied by $\mu^* = 0.6$, correspond to the same Coulomb stress changes as realized by means of the tangential loads. The solid line corresponds to maximum possible (instantaneous) clock advance. The large circles are plotted if the nucleation point appear outside of the Coulomb stress change area.

the whole fault, the clock advance is always positive, which means that earthquake occurs always earlier with respect to the regular behavior. On the other hand, in case of stressing at fault patches, for some CS load times the clock advance is negative, meaning that the earthquake is delayed although the applied CS is positive.

[19] The detailed analysis of the modeling results allows a qualitative explanation of the fault response to the heterogeneous CS load. The CS load causes sudden increase of slip velocities in the stressed region. Early in the earthquake cycle when the increase is not strong enough to invoke the major earthquake instability yet, only a smaller event initiates, rupturing only a small part of the whole fault with the largest slip velocities being several orders of magnitude below the threshold in our earthquake definition (1 mm/s). The resulting stress drop increases stress in the surrounding, which then results in a very slow (of the order of km/yr) wave-like progression of the slip velocity-stress disturbance from the CS load area along the fault. As the fault is in the background driven by the plate velocity, at some point the fault may or may not get repetitively again to an almost unstable regime, during which the largest slip velocities do not exceed 1 mm/s, causing again the stress release and generation of the slow slip velocity-stress wave. These effects give rise to a complicated spatial-temporal pattern of rate-and-state behavior, which results not only in the positive clock advance for the major earthquake but also in the negative one, with the nucleation area being not confined in the CS load region.

[20] Let us further examine the CS loads later in the earthquake cycle when the CS load results in slip velocity increase sufficient enough to initiate directly the major earthquake in the CS load area. As the nucleation point is not much sensitive to the depth of the CS increase area (Figure 3a), we arbitrarily select area of the same size as before but located in the middle depth of the fault. Figure 4a shows clock advance as a function of load time (480–490 years) for various values of the tangential stress load. Figure 4b shows equivalent results obtained for normal stress unload. Note that tangential and normal stress values assumed (see legend in Figures 4a and 4b) correspond to the same CS change (equation (1)), regarding $\mu = 0.6$. As one can see, the resulting clock advances are almost the same in both cases, which supports the finding by *Perfettini et al.* [2003] that the results are independent on how the CS load is realized. Note that this holds even for earlier CS load times.

[21] Figure 4 shows that the clock advance approaches the instantaneous triggering (represented by the solid line in Figure 4) when increasing the CS load time. The way how it approaches depends on the CS value: The lower is the CS value, the later the CS load has to be applied to trigger the earthquake almost instantaneously (within 1–2 months after the stress load). Figure 4 also shows, by larger circles, cases when the nucleation point lies outside of the CS change area. As one can see, for the cases of almost instantaneous triggering the nucleation point lies in the Coulomb change area (see also Figures 3a (middle) and 3a (right)).

4. Conclusions, Implications, and Limitations

[22] We have studied Coulomb stress (CS) triggering for a 3D quasi-dynamic rate-and-state continuous fault model. We have applied positive CS loading at various stages of the seismic cycle not only on the whole fault as done by *Perfettini et al.* [2003] (in 2D), but also on only parts of the fault. Note that the latter cases do not have simple equivalents in the spring-slider models, and, therefore, have to be solved numerically. We have discussed the resulting clock advance and the mutual position of the nucleation point and the CS load area.

[23] This issue is of interest for seismic hazard assessment due to triggered earthquakes (aftershocks). It is because the nucleation point position on the fault strongly affects the spatial distribution of strong ground motions. Without any knowledge of the nucleation point the hazard maps are symmetrical around the anticipated fault [*Gallovič and Brokešová*, 2008]. The present paper shows that the rate-and-state fault model can help in constraining the hazard calculations. Let us assume that a strong earthquake has occurred and increased Coulomb stress on some part of a nearby active fault. One may expect that within the next

two months (the period of an almost instantaneous triggering, see above) the nucleation point will be located in the strike extent of the CS increase area, independently on the CS load amplitude. Such constraint might significantly modify the (time-dependent) hazard maps due to, e.g., highly pronouncing directivity effect. After this 'favorable' period of the two months the anticipated fault may still be triggered (not almost instantaneously), but in this case it can nucleate anywhere, and, moreover, even later than without the positive CS load.

[24] The studied model is highly idealized. Among others, no other interaction effects (such as viscoelastic stress transfer, pore pressure changes, etc.) than the static elastic stress redistribution are assumed. The other simplifications are perfectly planar vertical strike-slip fault, almost homogeneous distribution of the friction parameters (a, b, α), constant normal stress, and homogeneous medium embedding the fault, etc. We also select only few particular cases of the CS load areas (in terms of position and size). Nevertheless, we have found some new features of the rate-and-state fault response to the heterogeneous Coulomb stress load. Our results have to be considered as exploratory and suggestive to seek evidences in real triggering sequences. This, however, goes beyond the extent of this paper, and is left for further studies.

[25] **Acknowledgments.** Jiří Zahradník and an anonymous reviewer helped to improve the manuscript. The work is a part of the following projects supported in the Czech Republic: GACR 205/07/0502, PostDoc GACR 205/08/P013, GAUK 279/2006/B-GEO/MFF, and MSM 0021620860.

References

Andrews, D. J. (1974), Evaluation of static stress on a fault plane from a green's function, *Bull. Seismol. Soc. Am.*, *64*, 1629–1633.

Dieterich, J. H. (1979), Modeling of rock friction: 1. Experimental results and constitutive equations, *J. Geophys. Res.*, *84*, 2161–2168.

Dieterich, J. H. (1994), A constitutive law for rate of earthquake production and its application to earthquake clustering, *J. Geophys. Res.*, *99*, 2601–2618.

Gallovič, F., and J. Brokešová (2008), Probabilistic aftershock hazard assessment II: Application of strong ground motion modeling, *J. Seismol.*, *12, 65–78.*

Gomberg, J., N. M. Beeler, M. L. Blanpied, and P. Bodin (1998), Earthquake triggering by transient and static deformations, *J. Geophys. Res.*, *103*, 24,411–24,426.

Linker, M. F., and J. H. Dieterich (1992), Effects of variable normal stress on rock friction: Observations and constitutive equations, *J. Geophys. Res.*, *97*, 4923–4940.

Perfettini, H., J. Schmittbuhl, and A. Cochard (2003), Shear and normal load perturbations on a two-dimensional continuous fault: 1. Static triggering, *J. Geophys. Res.*, *108*(B9), 2408, doi:10.1029/2002JB001804.

Press, W. H., B. P. Flannery, S. A. Teukolsky, and W. T. Vetterling (1992), *Numerical Recipes in Fortran: The Art of Scientific Computing*, 2nd ed., Cambridge Univ. Press, New York.

Rice, J. R. (1993), Spatio-temporal complexity of slip on a fault, *J. Geophys. Res.*, *98*, 9885–9907.

Roy, M., and C. Marone (1996), Earthquake nucleation on model faults with rate- and state-dependent friction: Effects of inertia, *J. Geophys. Res.*, *101*, 13,919–13,932.

Ruina, A. L. (1983), Slip instability and state variable fricton laws, *J. Geophys. Res.*, *88*, 10,359–10,370.

Scholz, C. H. (1998), Earthquakes and friction laws, *Science*, *391*, 37–42.

Steacy, S., J. Gomberg, and M. Cocco (2005), Introduction to special section: Stress transfer, earthquake triggering, and time-dependent seismic hazard, *J. Geophys. Res.*, *110*, B05S01, doi:10.1029/2005JB003692.

F. Gallovič, Department of Geophysics, Faculty of Mathematics and Physics, Charles University in Prague, V Holešovičkách 2, Praha 8, 180 00 Czech Republic. (gallovic@karel.troja.mff.cuni.cz)